Applied Catalysis A: General 514 (2016) 51–59

Contents lists available at ScienceDirect

Applied Catalysis A: General

journal homepage: www.elsevier.com/locate/apcata

Methanol synthesis from CO_2 and H_2 over $Pd/ZnO/Al_2O_3$: Catalyst structure dependence of methanol selectivity

Jinghua Xu[a,b], Xiong Su[a], Xiaoyan Liu[a], Xiaoli Pan[a], Guangxian Pei[a], Yanqiang Huang[a,*], Xiaodong Wang[a,*], Tao Zhang[a], Haoran Geng[c,**]

[a] State Key Laboratory of Catalysis, Dalian Institute of Chemical Physics, Chinese Academy of Sciences, No. 457 Zhongshan Road, Dalian 116023, China
[b] School of Materials Science and Engineering, Shandong University, No. 17923 Jingshi Road, Jinan 250061, China
[c] School of Materials Science and Engineering, Jinan University, No. 106 Jiwei Road, Jinan 250022, China

ARTICLE INFO

Article history:
Received 2 October 2015
Received in revised form
10 December 2015
Accepted 8 January 2016
Available online 13 January 2016

Keywords:
CO_2 hydrogenation
Methanol synthesis
Supported Pd catalyst
PdZn alloy

ABSTRACT

CO_2 hydrogenation to methanol was investigated over $Pd/ZnO/Al_2O_3$, focusing on the influence of the preparation method, reduction temperature and Pd loading on the catalytic performance. The structure of each catalyst was thoroughly examined using various techniques. The results indicated that the methanol selectivity depended on the content of PdZn alloy, which changed dynamically with varying the preparation methods and pretreatment procedures of the catalysts. More specifically, the ratio of $PdZn/Pd^0$ in the bimetallic compound increased with the rise of the reduction temperature, which eventually led to the increase of methanol selectivity. Additionally, the EXAFS results revealed the presence of ZnO_x modified Pd species when the Pd loading was decreased to be lower than 2 wt%. However, the CH_3OH selectivity remained almost identical when the reactions were conducted under similar CO_2 conversions. Therefore, we conclude that both the PdZn alloy and Pd modified by ZnO_x islands are the active sites for methanol synthesis from CO_2 hydrogenation.

1. Introduction

Recently, catalytic synthesis of methanol from CO_2 hydrogenation is receiving increasing attention, not only because methanol is a key platform chemical, but also because of its use as a promising chemical storage carrier for the excess H_2 generated from renewable energy and as a solution for greenhouse gas recycling [1–6]. This reaction would be economically and technically viable if CO_2 fixation could be carried out under mild conditions and the hydrogen gas could be manufactured on a large scale from renewable energy sources, such as solar energy, hydropower and biomass [7,8].

$$CO_2 + 3H_2 = CH_3OH + H_2O \Delta H = -49.43\,kJ/mol \quad (1)$$

As shown in Eq. (1), the thermodynamics of CO_2 hydrogenation reaction favors the formation of methanol at high pressure and low temperature. However, the kinetics of this reaction is slow. The activation of CO_2 occurs with a sufficient rate only at the temperature higher than 200 °C. Under such conditions, the formation of by-products (CO, hydrocarbons and alcohols) lowers the methanol selectivity and yield. Thus, the development of catalysts with high methanol selective is essential. Cu-based catalysts are used commonly; however, they still suffer from an instable drawback under higher reaction temperatures. Especially in batch-wise operation conditions, when the catalyst is exposed to an intermittent oxidizing atmosphere (likely, trace of O_2), the pyrophoric property of Cu as well as its ease of sintering, not only affects the service life, but also implies that once the catalyst is deactivated, it is destroyed permanently [9–16]. Pd-based catalysts are considered to be the potential candidates which possess good long-term stability and resistance to sintering [17–24]. Moreover, when Pd is oxidized into PdO, it can be reduced and restored to a functional state in situ. However, to our knowledge, the origin of active site in these catalysts is still under debate even though tremendous efforts have been made to identify it.

Up to now, several strategies have been employed for improving the efficiency of Pd ensembles by modifying the catalyst structure. The type of supports, including oxides (SiO_2, CeO_2, ZnO, etc.) [25–30] and multi-walled carbon nanotubes [31], the catalyst preparation methods, as well as the thermal treatment conditions, have strong effects on the particle size and the electronic

* Corresponding author. Fax: +86 411 84685940.
** Corresponding author. Fax: +86 531 82765314.
E-mail addresses: yqhuang@dicp.ac.cn (Y. Huang), xdwang@dicp.ac.cn (X. Wang), mse_genghr@ujn.edu.cn (H. Geng).

http://dx.doi.org/10.1016/j.apcata.2016.01.006
0926-860X/

properties of Pd entity, which are considered to be the critical factors affecting the performance of methanol synthesis. However, it is still unclear which factor predominantly influences the formation of active sites. Lee's group [32–34] reported that the catalytic performance was associated with ZnO_x islands located on the surface of Pd. This geometric microstructure could be achieved directly by a deposition–precipitation method of preparation or by relatively low-temperature reduction of a coprecipitated sample. Reduction or calcination at high temperature led to the formation of Pd–Zn alloy, but lost the catalytic performance. In contrast, Iwasa et al. [28] found that the turnover frequency and methanol selectivity were markedly larger on Pd/ZnO than those on Cu/ZnO type catalyst. It was proposed that, when the catalyst was reduced at high temperature, PdZn alloy was formed, which served as the active site for methanol synthesis. In agreement with this finding, Lebarbier [35] and Ota et al. [36] illustrated that PdZn particles were more active than Pd^0 for methanol synthesis. It is possible that the two seemingly contradictory viewpoints on the Pd electronic structure in catalytic activity discussion are both reasonable under their respective reaction conditions. The objective of this work is to systematically investigate the relationship between the catalyst structure and the performance in order to illustrate the original active sites for methanol formation.

In addition, although ZnO has been regarded as the most effective support for the Pd catalyst in CO_2 hydrogenation, it presents disadvantages of low surface area and poor structural stability. Commonly, incorporation of Al_2O_3 to prepare binary oxides is used to improve the catalytic performance. However, the preparation methods have a significant effect on the catalytic performance [37]. Hydrotalcite, containing transition metals, is receiving considerable attention as a catalyst precursor because large specific surface area and high dispersion of metallic particles are usually available after reduction in H_2 [38–42]. Therefore, in this work, Zn–Al hydrotalcite (ZnAl-HT) was prepared exclusively and used as the support for palladium. The influence of preparation method, reduction temperature and Pd loading of $Pd/ZnO/Al_2O_3$ on the catalytic performance of CO_2 hydrogenation to methanol was investigated. The catalysts structures were thoroughly characterized by HRTEM, XRD, in situ DRIFTS and XAS. The main purpose of the present study is to explore the influence of different pretreatment conditions that might optimize the catalyst formulation with high methanol selectivity.

2. Experimental

$Zn(NO_3)_2{\cdot}6H_2O$ (AR) and $Al(NO_3)_3{\cdot}9H_2O$ (AR) were purchased from Sinopharm Chemical Reagent Co., Ltd. NaOH (AR) and Na_2CO_3 (AR) were purchased from Tianjin Kermel Chemical Reagent Co., Ltd. Deionized water was used in all experiments. All chemicals were used as received without further purification.

2.1. Catalyst preparation

Zn–Al hydrotalcite was used as the precursor for preparing the $ZnO–Al_2O_3$ binary oxides support via a coprecipitation (CP) method as described elsewhere [43,44]. In a typical synthesis, required amount of $Zn(NO_3)_2{\cdot}6H_2O$ and $Al(NO_3)_3{\cdot}9H_2O$ were dissolved in 50 mL deionized water, with total molar concentrations of Zn^{2+} and Al^{3+} of 0.8 and 0.4 mol L^{-1}, respectively. This solution was added dropwise (3 mL min^{-1}) into another 50 mL mixed solution containing 4.24 g Na_2CO_3 and 2.40 g NaOH with continuous stirring. Afterwards, the pH value of the system was adjusted to 10 by introducing 3 mol L^{-1} NaOH aqueous solution and a white suspension was obtained. Then, the suspension was kept at 65 °C for 18 h with continual stirring to get a precipitate with hydrotalcite-like structure. The mixture was washed repeatedly with deionized water to remove sodium ions. Finally, the obtained sample was dried at 60 °C for 12 h.

x wt% $Pd/ZnO/Al_2O_3$ catalysts with different Pd loadings (*x* = 0.5, 2, 5) were synthesized by a deposition–precipitation (DP) method. Take the 5 wt% $Pd/ZnO/Al_2O_3$ catalyst for example, 1.0 g Zn–Al hydrotalcite was dispersed into 100 mL deionized water with ultrasonic assistant. An adequate amount of $PdCl_2$ solution (4.39 mL, containing 52.7 mg Pd) was added into the suspension with magnetic stirring. Then, the PH value of the solution was adjusted to 9. The mixture was kept in a water bath at 60 °C and stirred for 3 h. The as-obtained deposit was washed with deionized water to remove sodium and chloride ions, then dried at 60 °C and reduced at 300 °C for 1 h in a pure hydrogen flow. Other catalysts with varied Pd contents were synthesized as described above.

In order to examine the effect of preparation methods on the catalytic performance, another two different methods were employed to synthesize the 5 wt% Pd $Pd/ZnO/Al_2O_3$ catalysts.

Coprecipitated catalyst was prepared by a method similar to that of Zn–Al hydrotalcite. The molar ratio of Pd^{2+}, Zn^{2+} and Al^{3+} was 0.1:2:1, with a total concentration of 0.4 mol L^{-1} in 50 mL aqueous solution. This solution was added dropwise into 50 mL mixed alkali solution containing 0.04 mol Na_2CO_3 and 0.06 mol NaOH. The following experiment steps were performed according to the procedures described above.

Impregnated catalyst (IM) was synthesized using Zn–Al hydrotalcite as the support. Briefly, 1 g Zn–Al hydrotalcite was added into a $Pd(NO_3)_2{\cdot}2H_2O$ solution (5 mL, containing 52.5 mg Pd), followed by aging at room temperature for 2 h. Then, the sample was dried at 60 °C for 12 h, and calcined in air at 300 °C for 2 h.

2.2. Activity test

The methanol synthesis reaction was evaluated in a continuous-flow fixed-bed reactor. Typically, the catalyst (20–40 mesh, 0.5 g), diluted with SiO_2 (20–40 mesh, 2 g), was loaded into a stainless steel tubular flow reactor (i.d. 6 mm). Prior to the activity tests, the catalyst was reduced at different temperatures (300 and 500 °C) for 1 h in pure hydrogen at a flow rate of 20 mL min^{-1} under atmospheric pressure. The activity was measured at 180–220 °C, 3.0 MPa, GHSV = 3600 mL h^{-1} g^{-1} and a feed (a $H_2/CO_2/N_2$ mixture, H2VCO2/N2 = 69/23/8) flow rate of 30 mL min^{-1}. The effluent gas products were kept at 120 °C to prevent any condensation, and then analyzed on-line using an Agilent 6890 gas chromatograph equipped with dual detectors (TCD and FID) and dual columns filled with carbon molecular sieve (TDX-01) and FFAP, respectively. The former column (2.0 m × 2 mm) was used for the analysis of N_2 (used as internal standard gas), CO and CO_2; the latter (30.0 m × 0.32 mm × 1.0 μm) one was used for the analysis of CH_4 and CH_3OH.

The catalytic performance was expressed by the CO_2 conversion and CH_3OH selectivity, which were calculated based on the difference between the concentrations of components at the inlet and outlet.

The CO_2 conversion was defined as:

$$\text{Conversion}(CO_2\%) = \frac{CO_2(\text{in}) - CO_2(\text{out}) \times \frac{N_2(\text{in})}{N_2(\text{out})}}{CO_2(\text{in})} \times 100\%$$

The carbon-based selectivity was defined as:

$$\text{Selectivity}(CH_3OH\%) = \frac{CH_3OH(\text{out})}{CH_3OH(\text{out}) + CO(\text{out}) + CH_4(\text{out})} \times 100\%$$

$$\text{Selectivity}(CO\%) = \frac{CO(\text{out})}{CH_3OH(\text{out}) + CO(\text{out}) + CH_4(\text{out})} \times 100\%$$

$$\text{Selectivity}(CH_4\%) = \frac{CH_4(\text{out})}{CH_3OH(\text{out}) + CO(\text{out}) + CH_4(\text{out})} \times 100\%$$

where x (in) (x stands for CO_2, CO, CH_3OH, N_2 and CH_4) corresponds to the *x* concentrations at the inlet, and x (out) represents the *x* concentrations at the outlet. Methanol and CO were the main products observed, along with traces (less than 1%) of methane. Therefore, we did not pay attention to CH_4 selectivity in the following study.

2.3. Catalyst characterizations

Thermo IRIS Intrepid II Inductively Coupled Plasma (ICP) was used to determine the content of Pd in the catalysts. X-ray diffraction (XRD) measurements were carried out using a PANalytical X'Pert-Pro powder X-ray diffractometer with CuKα monochromatized radiation (λ = 0.1541 nm). The voltage and current were operated at 40 kV and 40 mA, respectively. A continuous-scan mode was used to collect 2θ data from 10° to 90°, at scanning speed of 4° min^{-1}. High-resolution scanning transmission electron microscopy (HRSTEM) images were recorded using a JEM-2100F field emission electronic microscope equipped with a STEM dark-field detector. The accelerating voltage was 200 kV.

Temperature-programmed reduction (TPR) experiments were conducted using a Micromeritics AutoChem II 2920 Automated Catalyst Characterization System. Prior to the experiment, the sample (about 100 mg) was loaded into a U-shaped quartz reactor and pretreated with Ar at 150 °C for 1 h to remove adsorbed water. After cooling to −50 °C, 5 vol% H_2/N_2 mixed gas was passed into the sample, and then heated to 900 °C at a ramping rate of 10 °C min^{-1}. The dispersion of Pd was measured by a hydrogen–oxygen titration method. The samples were reduced in-situ under the same condition as for the activity test. Then, the freshly reduced catalysts were flushed with Ar for 30 min at the reduction temperature in order to remove extra hydrogen adsorbed on the surface. When the temperature was decreased to 120 °C, 2% O_2/He was passed through the catalysts and maintained for 0.5 h. Then, pure H_2 was injected until the system was saturated. The amount of H_2 adsorbed was calculated from the pulse results, monitored using a thermal conductivity detector (TCD). The metal dispersion was calculated from the H_2 adsorption results by assuming adsorption of three H atoms per Pd atom.

In situ diffuse reflectance infrared Fourier transform (DRIFT) spectra of CO adsorption was collected on a BRUKER Equinox 55 spectrometer equipped with a MCT detector, operated at a resolution of 4 cm^{-1}. Before the experiment, all the samples were reduced in situ with H_2 at a flow rate of 20 mL min^{-1} for 1 h. Then, the flowing gas was switched to helium at the same temperature and cooled down to room temperature. After the pretreatment, a background spectrum was collected based on 80 scans; this was automatically subtracted from the measured spectra. The CO adsorption experiments were carried out subsequently. 1% CO in He was introduced into the reaction cell at a total flow rate of 20 mL min^{-1} for about 30 min, followed by purging with pure He (20 mL min^{-1}) for 30 min. Finally, the spectra were collected.

X-ray absorption near-edge structure (XANES) and extended X-ray absorption fine structure (EXAFS) spectra at the Pd K-edge were obtained at the BL14W1 at the Shanghai Synchrotron Radiation Facility (SSRF), Shanghai institute of applied physics (SINAP), China. A double Si (311)—crystal monochromator was employed for energy selection. Energy calibration was done using Pd foil. Before the experiments, the samples were reduced at different temperatures and sealed with Kapton films in a glove box. The spectra were collected at room temperature. For the 2 wt% Pd and 0.5 wt% Pd samples, a fluorescence mode was used with solid state detector, while a transmission mode was employed for all the other samples. The Athena software package was used to analyze the data.

The content of PdZn alloy was estimated by comparing the coordination numbers (N_{Pd-Zn} and N_{Pd-Pd}), which were obtained from the fit with the theoretical values. If all Pd presented as PdZn alloy, the ratio of N_{Pd-Zn}/N_{Pd-Pd} would equal two. Therefore, the calculation formula was defined as:

$$\text{Content}(PdZn) = \frac{N_{Pd-Zn}/N_{Pd-Pd}}{2} \times 100\%$$

Table 1
The effect of supports and preparation methods on CO_2 hydrogenation over Pd-based catalysts.

Catalysts	Preparation methods	C_{CO_2}%	S_{CH_3OH}%	Y_{CH_3OH}%
5 wt% Pd/ZnO	DP	2.5	72.2	1.8
5 wt%	DP	2.9	79.4	2.3
$Pd/ZnO/Al_2O_3$	IM	0.6	65.9	0.4
	CP	1.3	86.0	1.1

Note: Catalysts reduced in H_2 at 300 °C for 1 h, 0.5 g catalyst, T = 180 °C, P = 3 MPa, $H_2/CO_2/N_2$ = 69:23:8, flow rate = 30 mL min^{-1}; data collected after 3 h on line.

3. Results and discussion

3.1. Effect of the support and preparation method

It has been previously reported that the activity and selectivity of Pd catalysts for methanol synthesis from CO_2 and H_2 depend on the type of supports [25–27]. Among all the investigated Pd-based catalysts, Pd/ZnO exhibited the highest activity and methanol selectivity [28]. In this work, by replacing ZnO support with the ZnO/Al_2O_3 (prepared from hydrotalcite precursor), we found that both the CO_2 conversion and CH_3OH selectivity increased from 2.5% to 2.9% and 72.2% to 79.4%, respectively (see Table 1). One possible reason for the enhanced performance is that the binary oxide support possess higher surface area than that of ZnO (S_{BET} of ZnO is 2.8 m^2 g^{-1}, S_{BET} of ZnAl-HT is 43.4 m^2 g^{-1}), which favors the dispersion of metallic active sites. The other is that Al_2O_3 is not only a structural promoter but also an electronic one [45].

The influence of preparation methods of $Pd/ZnO/Al_2O_3$ catalyst on the catalytic performance was further investigated. As shown in Table 1, the highest methanol selectivity of 86.0% was obtained over the CP-catalyst (catalyst prepared by CP method). The selectivities over the IM-catalyst (catalyst prepared by IM method) and DP-catalyst (catalyst prepared by DP method) were 65.9% and 79.4%, respectively. However, the CO_2 conversion over the CP-catalyst reached only half of that over the DP-catalyst. Moreover, the IM-catalyst exhibited the lowest CO_2 conversion of 0.6% among all the three samples. These prominent discrepancies in performance may be originated from the variable formation pathways of active sites and their accessibility. For instance, a homogeneous distribution of Pd and Zn species in the precipitate was achieved by CP method, which favored the formation of single PdZn alloy phase after reduction in H_2 [46]. These highly dispersed PdZn particles were responsible for the high CH_3OH selectivity. However, the drawback of this preparation method is that considerable amounts of active sites were embedded in the catalyst interior, which reduced the CO_2 conversion. For the IM method, the support was partially soluble in the acidic Pd nitrate aqueous (used as the Pd precursor for impregnation), after drying, calcination and reduction treatments, the originally dissolved ions deposited again on the metal particles. Therefore, both the CO_2 conversion and methanol selectivity over the IM-catalyst were decreased due to the alternation of the textural properties [47]. Therefore, in order to obtain both high methanol selectivity and yields, DP method was selected to prepare the catalysts in the following study.

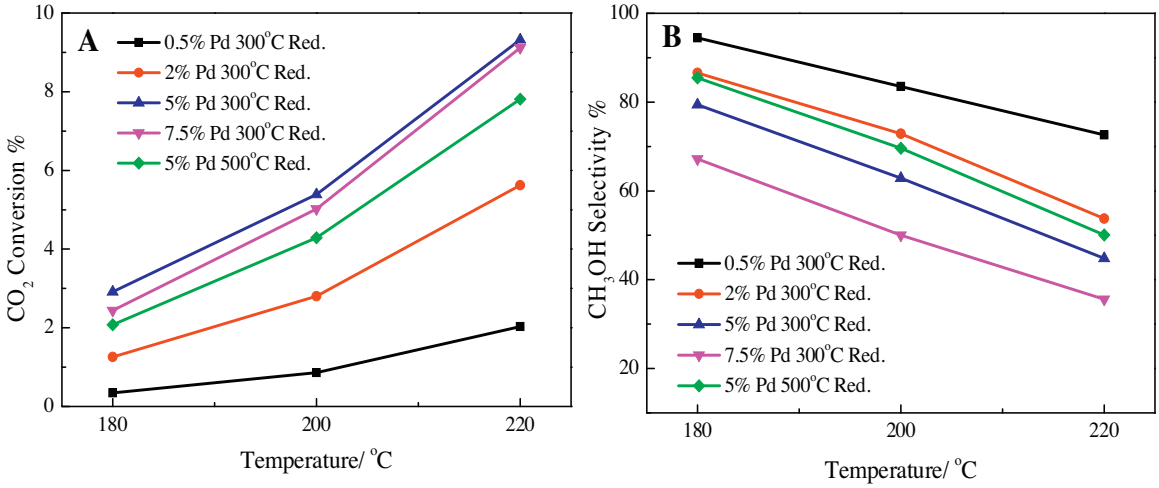

Fig. 1. (A) CO_2 conversion, (B) CH_3OH selectivity as a function of reaction temperature over the 0.5 wt%, 2 wt%, 5 wt% and 7.5 wt% $Pd/ZnO/Al_2O_3$ catalysts reduced at 300 °C or 500 °C. Catalysts reduced in H_2 for 1 h, 0.5 g catalyst, T = 180–220 °C, P = 3 MPa, $H_2/CO_2/N_2$ = 69:23:8, flow rate = 30 mL min^{-1}; data collected after 3 h on line.

3.2. *Effect of the reduction temperature*

Fig. 1 shows the CO_2 conversion and CH_3OH selectivity over $Pd/ZnO/Al_2O_3$ catalysts reduced at 300 and 500 °C in the reaction temperature range of 180–220 °C. The results indicated that the CO_2 conversion decreased slightly when the reduction temperature was increased from 300 to 500 °C, probably due to the increased particle size of Pd species. On the contrary, the trend in the CH_3OH selectivity was increased. Obviously, this result indicates that higher reduction temperature favors the selectivity toward methanol. To clarify the origin of the selectivity behavior, the catalyst structures were characterized systematically.

The phase composition of the 5 wt% $Pd/ZnO/Al_2O_3$ catalysts reduced at 300 and 500 °C was investigated by powdered X-ray diffraction. As shown in Fig. 2, the XRD pattern exhibits only one wide bandwidth peak at $2\theta = 41.25°$ for the reflection of PdZn (1 1 1) crystal plane when the catalyst reduced at 300 °C. However, we cannot rule out the presence of Pd particles because of the poor resolution of the broad peak. With the reduction temperature rising to 500 °C, the XRD pattern shows two intense peaks at $2\theta = 41.25°$ and 44.13°, reflecting the existence of PdZn alloy phase with (1 1 1) and (200) crystal planes. Using Scherrer's equation, we obtained that the crystal size of PdZn particles were 9.5 nm and 17.0 nm for the catalysts reduced at 300 and 500 °C, respectively.

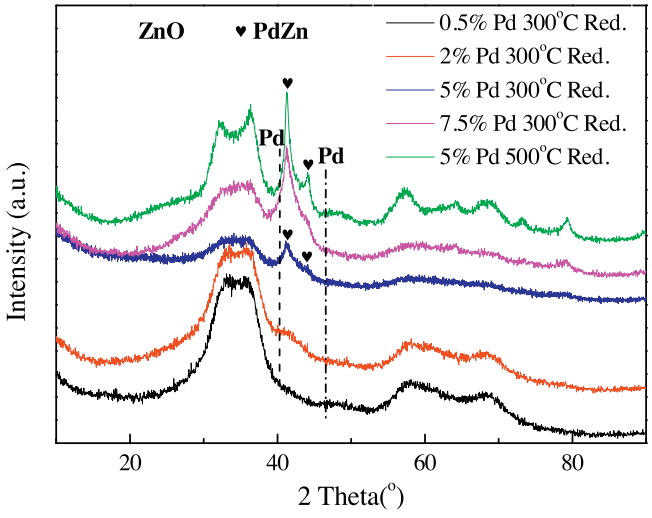

Fig. 2. XRD patterns of the 0.5 wt%, 2 wt%, 5 wt% and 7.5 wt% $Pd/ZnO/Al_2O_3$ catalysts reduced at 300 °C or 500 °C.

The structures of $Pd/ZnO/Al_2O_3$ catalysts reduced at 300 °C and 500 °C were further examined by TEM. As shown in Fig. 3A and C, highly dispersed and small-sized nanoparticles were observed in the STEM–HAADF images. The average particle size of Pd species obtained from the projected areas were estimated to be 3.9 ± 0.9 nm and 4.3 ± 1.3 nm for the catalysts reduced at 300 °C and 500 °C respectively, which were much smaller than those obtained from the XRD results. The reason is assumed that quite an amount of small particles (<2 nm) were beyond the detection limit of XRD technique. HRSTEM images were used to identify the crystal structure of the PdZn nanoparticles (ICDD 06-0620). As shown in the amplified image (Fig. 3B), the lattice fringe size was 2.2 Å, corresponding to the PdZn (1 1 1) and (1 – 1) lattice distance (theoretical spacing: 2.18 Å), with a characteristic angle of 64.6°. A smaller lattice fringe of 2.0 Å was also visible, corresponding to the PdZn (0 2 0) lattice distance (theoretical spacing: 2.05 Å) [48,49]. Fig. 3D displays the HRSTEM image of the catalyst reduced at 500 °C, which performs a higher resolution. The microstructure was confirmed to be identical to that in the catalyst reduced at 300 °C. Based on these results, the crystalline phase of the PdZn particles was identified as tetragonal. The related fast Fourier transformation pattern further confirms this conclusion.

DRIFTS of CO adsorption under room temperature was employed to determine the surface properties of the metallic Pd and PdZn components over the 5 wt% $Pd/ZnO/Al_2O_3$ catalyst. As shown in Fig. 4, the band appeared at 2054 cm^{-1} on the catalyst reduced at 50 °C was attributed to the vibration of linearly adsorbed CO on Pd^0. In addition, the other band situated at 1940 cm^{-1} was the characteristic of bridge-bonded CO on Pd^0. Besides the band of 2054 cm^{-1}, there appeared another band situated at 2087 cm^{-1} for the catalyst reduced at 300 °C. According to the previous results [50–52]. this band was attributed to the vibration of linearly adsorbed CO on PdZn alloy. The other band situated at 1919 cm^{-1} with a shoulder at 1970 cm^{-1} was the characteristic of bridge-bonded CO adsorbed on Pd^0. This result indicates the coexistence of monometallic Pd and PdZn alloy. However, when the reduction temperature was increased to 500 °C, the bands became too weak to obtain any useful information about the surface composition.

XAS is a powerful technique for revealing the structural and chemical state of nanoparticles. Fig. 5A shows the normalized Pd K-edge XANES spectra of the $Pd/ZnO/Al_2O_3$ catalysts reduced at 300 °C and 500 °C. Palladium foil was used as the reference material.

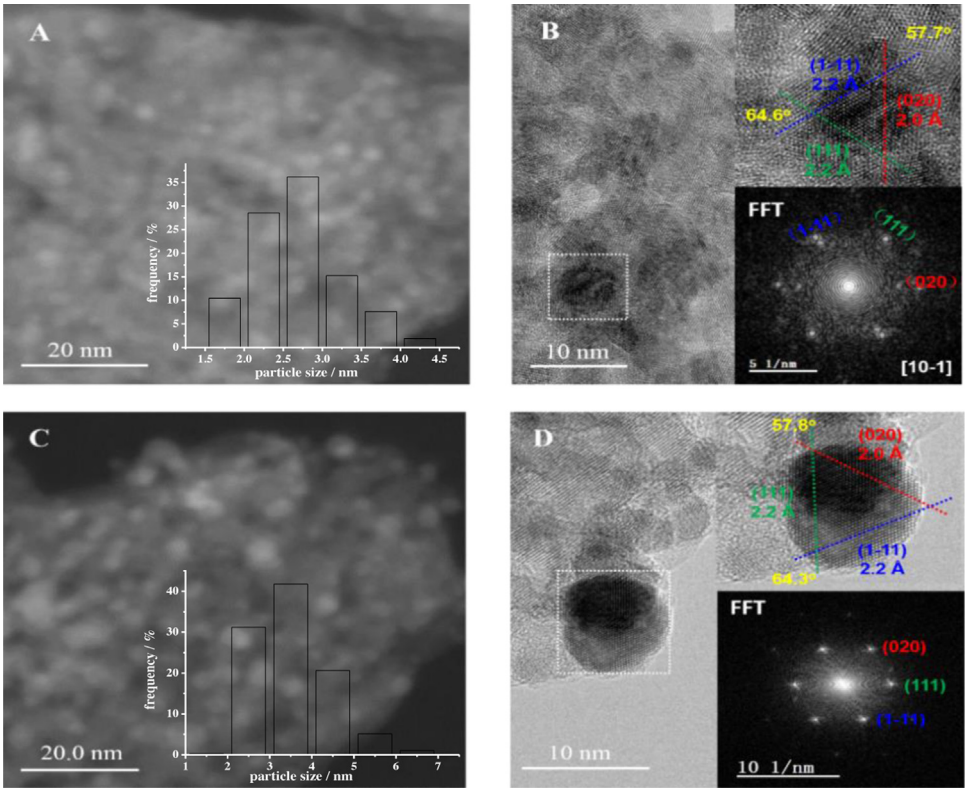

Fig. 3. STEM, HRTEM images and corresponding FFT patterns of the 5 wt% Pd/ZnO/Al_2O_3 catalyst reduced at: (A and B) 300 °C and (C and D) 500 °C, respectively.

The peak intensities in the near-edge spectra reflected the oxidation state of Pd in different samples. The spectra of both two catalysts were similar to that of Pd foil, suggesting that the Pd species were fully reduced [53,54]. Fig. 5B shows the Fourier transforms of the Pd k^3-weighted EXAFS spectra of the Pd foil and the catalysts. Obviously, the first nearest neighbor distance of Pd/ZnO/Al_2O_3 catalysts was shorter than the Pd-Pd bond length, implying the existence of Pd—Zn bond [32,55,56]. The curve fitting results are listed in Table 2. It has been reported that in Pd foil, the Pd–Pd coordination number (CN) was 12.0, with a bond distance of 2.75 Å; while in an ordered 1:1 PdZn alloy, the Pd–Pd and Pd–Zn coordination numbers were 4 and 8, with the bond distance of 2.90 Å and 2.60 Å, respectively [56,57]. As shown in Table 2, PdZn alloy was already formed on the catalyst reduced at 300 °C, which included a contribution of the Pd—Zn bond distance (R_{Pd-Zn}) of 2.59 Å and a coordination number (N_{Pd-Zn}) of 3.5. The Pd—Pd bond distance (R_{Pd-Pd}) was 2.70 Å, and the coordination number (N_{Pd-Pd}) was 5.1. The ratio between metallic Pd and alloyed Pd in PdZn could be estimated by comparing the coordination numbers of N_{Pd-Zn} and N_{Pd-Pd} obtained from the fitting results. If all Pd presented as PdZn alloy, the ratio of N_{Pd-Zn}/N_{Pd-Pd} would be equal to two. Therefore, by calculating the fitting data of the catalyst reduced at 300 °C, approximately 34% of the Pd atoms presented in the form of PdZn alloy and 66% of the Pd atoms were in the metallic state, which corresponded to a N_{Pd-Zn}/N_{Pd-Pd} ratio of 0.69. In addition, we noted that the sum of the *CN* of Pd–Pd and Pd–Zn bonds was 8.6, which was smaller

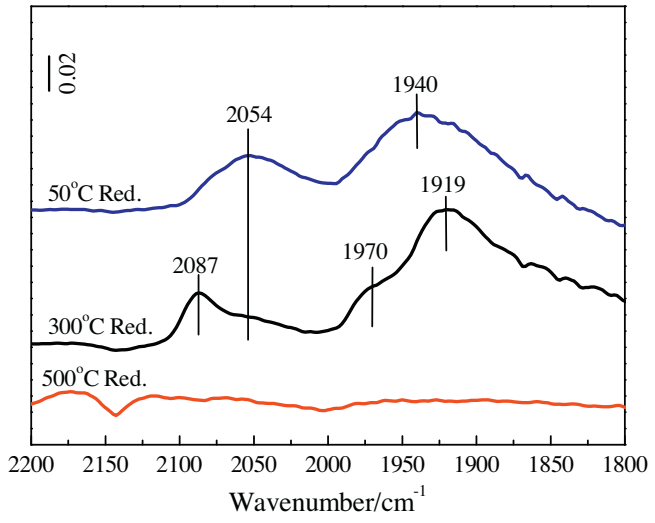

Fig. 4. DRIFT spectra of CO adsorption on the 5 wt% Pd/ZnO/Al_2O_3 catalyst with a reduction treatment at 50 °C, 300 °C and 500 °C for 1 h.

Table 2
EXAFS fitting data of the 0.5 wt%, 2 wt% and 5 wt% Pd/ZnO/Al_2O_3 catalysts reduced at 300 °C or 500 °C for 1 h.

Samples	Shell	*N*	*R* (Å)	$\sigma^2 \times 10^2$ (Å^2)	ΔE_0 (eV)	r-factor (%)
Pd foil	Pd–Pd	12.0	2.74	0.46	−6.2	0.40
5 wt% Pd 500 °C red.	Pd–Zn	7.3	2.60	0.84	−8.4	0.17
	Pd–Pd	3.6	2.87	1.05	−5.9	
5 wt% Pd 300 °C red.	Pd–Zn	3.5	2.59	0.85	−11.2	0.30
	Pd–Pd	5.1	2.70	0.85	−11.2	
2 wt% Pd 300 °C red.	Pd–O	0.8	1.97	0.48	−10.4	0.60
	Pd–Zn	2.9	2.58	0.96	−10.4	
	Pd–Pd	3.6	2.68	0.96	−10.4	
0.5 wt% Pd 300 °C red.	Pd–O	0.7	1.97	0.55	−12.0	0.45
	Pd–Zn	3.1	2.56	1.11	−12.0	
	Pd–Pd	3.3	2.67	1.11	−12.0	

N—the coordination number for the absorber–backscatterer pair. *R*—the average absorber–backscatterer distance. σ^2—the Debye–Waller factor. ΔE_0—the inner potential correction. The accuracies of the above parameters were estimated as $N = \pm 20\%$; $R = \pm 1\%$; $\sigma^2 = \pm 20\%$; $\Delta E_0 = \pm 20\%$. The data range used for data fitting in *k*-space (Δk) and *R*-space (ΔR) are 3.1–11.8 Å^{-1} and 1.2–3.1 Å, respectively.

than that of Pd foil, indicating that Pd was highly dispersed on the support [58], in good agreement with the TEM result. When the reduction temperature was increased to 500 °C, the Pd–Pd coordination number decreased to 3.6, while that of Pd–Zn increased to 7.3. The R_{Pd-Pd} elongated to about 2.87 Å, while the R_{Pd-Zn} remained at around 2.60 Å. Both the two bond distances were very close to those in the intermetallic PdZn alloy. The N_{Pd-Zn}/N_{Pd-Pd} ratio of 2 suggested that the PdZn alloy was formed with a face-centered tetragonal structure. This result provides a direct evidence of the complete transformation of Pd into PdZn alloy when the catalyst reduced at 500 °C.

To summarize this section briefly, the XRD (Fig. 2) and HRTEM (Fig. 3) results provided direct evidences of the formation of PdZn alloy upon the reduction of $Pd/ZnO/Al_2O_3$ catalyst. In situ DRIFT spectra revealed that the catalyst reduced at 300 °C contained both monometallic Pd and PdZn alloy, and the content of PdZn alloy was estimated to be 34% based on the XAS analysis. The metallic Pd was completely transformed into PdZn alloy when the reduction temperature was increased to 500 °C, which was accompanied by an increase in methanol selectivity (see Fig. 1B and Table 3). For example, the CH_3OH selectivity at 180 °C was 79.4% over the catalyst reduced at 300 °C, while this value increased to 85.5% when the reduction temperature was raised to 500 °C. The change in selectivity could be explained by the successive transformation of metallic Pd into PdZn alloy. It was proposed that during the Pd/ZnO reduction, PdO is first reduced, and then the adjacent ZnO is reduced to form PdZn alloy [59–61]. The higher the reduction temperature was, the greater extent of alloy would be formed, and hence the enhanced methanol selectivity.

3.3. Effect of the Pd loading

The influence of the Pd loading on the catalytic performance was investigated. Prior to the experiment, the content of Pd was determined by ICP spectrophotometry. The results showed that the measured Pd loadings were slightly smaller than that of the nominal composition (Table 4). It can be noted from Fig. 1 that the decrease in Pd loading led to an increase in CH_3OH selectivity, albeit at the expense of CO_2 conversion. We further compared the CH_3OH selectivity over the 2 wt%, 5 wt% and 7.5 wt% Pd/ZnAl-HT catalysts with reactions conducted under similar CO_2 conversion levels by verifying the space velocity. As shown in Table S1, the CH_3OH selectivities over all catalysts were within a similar range.

The TOF values (calculated on the basis of the number of surface Pd atoms on the ZnO/Al_2O_3 support) of the catalysts with varied Pd loadings were obtained by determining the Pd dispersion using hydrogen–oxygen titration method. The data in Tables 3 and 4 show that the Pd dispersion decreased with increasing the Pd loading. At the same reaction temperature, i.e., at 220 °C, the calculated TOF values increased slightly from 0.75×10^{-2} to 1.07×10^{-2} s^{-1} when the Pd loading decreased from 5 wt% to 0.5 wt%. The apparent activation energies (E_a) of CO_2 hydrogenation over these catalysts were also estimated, as shown in Fig. S1. The estimated E_a values over the 5 wt% and 2 wt% $Pd/ZnO/Al_2O_3$ catalysts were 59.9 and 64.8 kJ/mol, respectively, very close to those reported previously [31,36]. However, the estimated E_a value over the 0.5 wt% $Pd/ZnO/Al_2O_3$ catalyst was 71.5 kJ/mol, slightly higher than that over other catalysts. Since E_a was calculated based on CO_2 conversion, which contained both the methanol synthesis and the rWGS reaction. The higher E_a value estimated over the 0.5 wt% catalyst than that estimated over the 5 wt% and 2 wt% catalysts might be attributed to the decreased CO formation rate through rWGS reaction.

The stability experiment was tested over the 5 wt% $Pd/ZnO/Al_2O_3$ catalyst reduced at 300 °C. After 36 h time on stream at 200 °C, no deactivation was observed in either the CO_2 conversion or the CH_3OH selectivity (see Fig. S2), indicating that the catalyst possessed high stability.

To further study the effect of Pd loading on the catalytic performance, the detailed structures of these catalysts were examined. As shown in Fig. 2, the PdZn phase could only be observed at $2\theta = 41.23°$ (indicating the (1 1 1) lattice plane) over the samples with Pd loadings above 2 wt%. Reducing the Pd loading led to a decrease in peak intensity. For the catalysts with Pd loadings lower than 2 wt%, the PdZn phase was not detectable, likely due to the fact that the crystal size of PdZn was less than 2 nm, which was beyond the detection limit of XRD technique.

H_2-TPR profiles of the $Pd/ZnO/Al_2O_3$ catalysts with different Pd loadings were depicted in Fig. 6. In most cases, the peaks below 80 °C for all catalysts were ascribed to the reduction of PdO to metallic Pd [62,63]. The amount of H_2 consumption was calculated. The results showed that PdO could be completely reduced at such temperatures. Meanwhile, a small amount of ZnO species was also reduced. The ZnO/Al_2O_3 support was also detected as reference. It was found that the ZnO species started to be reduced at 602 °C on bare ZnO/Al_2O_3 support, but this peak shifted to 562 °C and even low temperatures when Pd was supported on the surface of ZnO/Al_2O_3, which can be ascribed to the spillover of hydrogen species from Pd to the support [64]. To be noted, the hydrogen consumption peaks appeared at high temperatures (>763 °C) over the Pd supported catalysts were resulted from the surface reaction (methanation or rWGS) of H_2 with CO_2, which derived from the decomposition of the interlayer carbonates [36,65].

The curve-fitting results of EXAFS spectra were summarized in Table 2, which provided the evidence of coexistence of Pd^0 and PdZn. Moreover, we found that a small amount of Pd–O species coexisted in the 0.5 wt% and 2 wt% Pd catalysts. The H_2-TPR results indicated that PdO species could be completely reduced to metallic Pd below 80 °C. Therefore, the Pd–O species existed in the 0.5 wt% and 2 wt% Pd catalysts were possibly resulted from the migration of partially reduced ZnO_x onto the surface of Pd particles at the interface [32]. A further reduction of the catalyst at higher temperatures led to the formation of PdZn alloy, possibly in a pathway like $Pd/ZnO \rightarrow Pd(H_y)/ZnO \rightarrow Pd(H_y)/ZnO_x/ZnO \rightarrow PdZn/ZnO$. Based on this assumption, three kinds of Pd-containing species were identified in these catalysts: Pd in PdZn alloy, Pd modified by ZnO_x and unaffected Pd^0. However, the ratio of these Pd-containing species couldn't be directly determined with XAFS characterization, due to the existence of Pd–O band.

In summary of this section, the XRD results indicated that the particle size of Pd species decreased with decreasing the Pd loading. In addition to PdZn alloy, the EXAFS results further revealed that ZnO_x islands modified Pd species formed when the Pd loading was less than 2 wt%. However, the CH_3OH selectivity remained nearly the same when the reaction was conducted under similar CO_2 conversions. Therefore, it arrived at a conclusion that Pd modified by ZnO_x islands was also the active site for methanol synthesis.

Various hypotheses for the reaction mechanism have been presented during the past decades; however, there is still controversy over some important issues. One of the major dispute topics is related to whether methanol synthesis and RWGS reactions are evolving in parallel pathways, sharing a common intermediate, or whether the methanol formation proceeds by sequential RWGS and CO hydrogenation reactions. By conducting H/D exchange experiments, Kunkes et al. [66] proved that the methanol synthesis and RWGS reactions proceeded on different surface sites in a parallel manner. It was reported that, for the steam reforming of methanol (MSR, the reverse reaction of methanol synthesis from CO_2 and hydrogen), the selectivity of the Pd catalysts was significantly enhanced upon the formation of Pd alloys such as, Pd–Zn, Pd–Ga and Pd–In by the reduction of Pd/ZnO, Pd/Ga_2O_3 and Pd/In_2O_3 [67,68]. Lin et al. [69] reported several possible pathways of MSR

Table 3
A comparison of the catalytic performance over all catalysts.

Catalyst	T_{red} (°C)	CO_2 conversion (%)		CH_3OH selectivity (%)		CO selectivity (%)		TOF × 10^{-2} (S)	
		220	200	220	200	220	200	220	200
0.5% Pd	300	2.0	0.86	72.6	83.5	27.3	16.2	1.07	0.45
2% Pd	300	5.6	2.8	53.7	72.9	46.2	27.0	0.85	0.43
5% Pd	300	9.3	5.4	44.8	62.9	55.1	37.1	0.75	0.40
7.5% Pd	300	9.1	5.0	35.6	50.0	64.4	49.9	1.07	0.38
5% Pd	500	7.8	4.3	50.1	69.6	49.9	30.3	1.37	0.76

Note: Catalysts reduced in H_2 for 1 h, 0.5 g catalyst, T = 180–200 °C, P = 3 MPa, $H_2/CO_2/N_2$ = 69:23:8, flow rate = 30 mL min^{-1}; data collected after 3 h on line. TOF = moles of CO_2 converted/(number of active centers × time of reaction). The number of active centers was determined by hydrogen–oxygen titration.

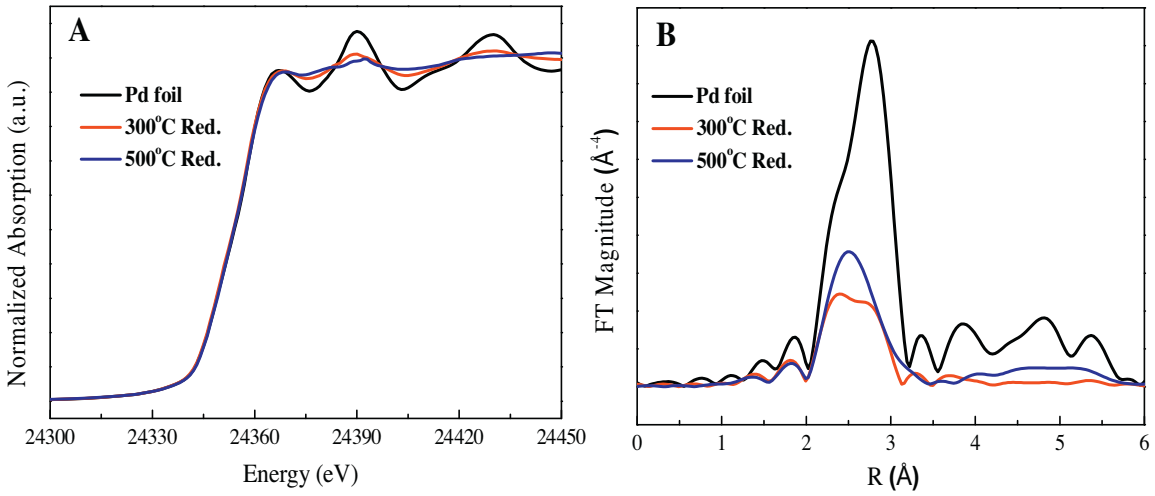

Fig. 5. (A) The normalized XANES spectra at Pd K-edge, (B) the corresponding Fourier transform of k^3-weighted EXAFS spectra for Pd foil and 5 wt% $Pd/ZnO/Al_2O_3$ catalysts reduced at 300 °C and 500 °C for 1 h.

Table 4
A comparison of the characteristics of all catalysts.

Catalyst	Reduction temperature (°C)	ICP:Pd (%)	Pd dispersion (%)	Particle size (nm)
0.5% $Pd/ZnO/Al_2O_3$	300	0.46	44.8	2.1 ± 0.6
2% $Pd/ZnO/Al_2O_3$	300	1.83	38.9	2.5 ± 0.5
5% $Pd/ZnO/Al_2O_3$	300	4.73	28.6	2.7 ± 0.6
7.5% $Pd/ZnO/Al_2O_3$	300	7.15	19.7	2.7 ± 0.6
5% $Pd/ZnO/Al_2O_3$	500	4.73	13.1	3.5 ± 0.9

Note: The average particle size of Pd species were estimated from the STEM images.

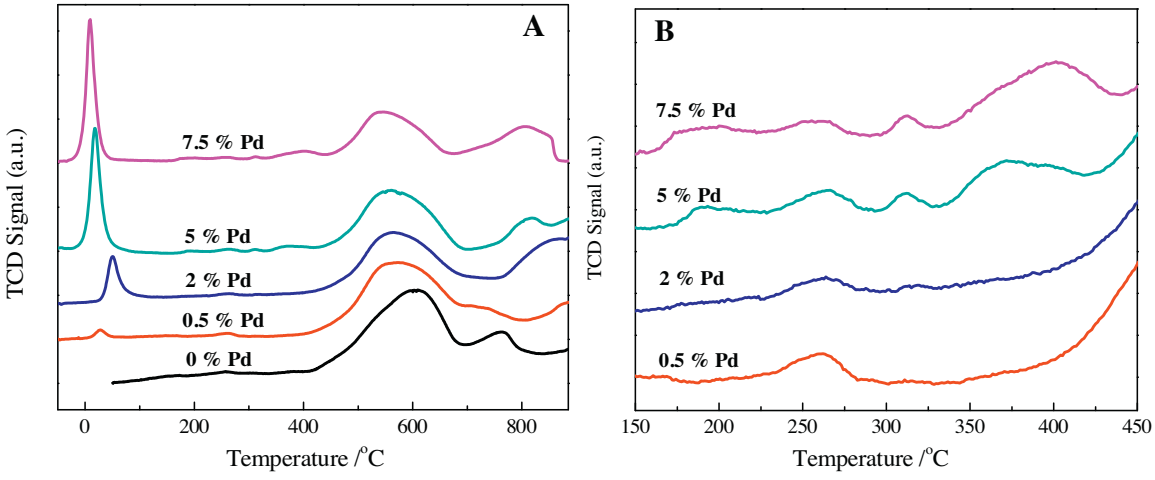

Fig. 6. H_2-TPR profiles of the $Pd/ZnO/Al_2O_3$ catalysts with different Pd loadings.

over PdZn alloy by using a plane-wave density functional theory. They found that formaldehyde was the key intermediate since the abstraction of one H atom from formaldehyde led to the CO pathway, while a reaction with adsorbed OH led to the formation of CO_2. The decomposition of formaldehyde into –CHO and further to CO was calculated to be kinetically favorable on Pd (1 1 1); whereas the reaction with hydroxyl group to the formation of CO_2 was more favorable on PdZn (1 1 1). Similarly, the high selectivity observed in methanol synthesis over the $Pd/ZnO/Al_2O_3$ catalyst might be attributed to the presence of Zn, while its effect on RWGS is less important. The critical role of Zn in CO_2 hydrogenation to methanol is also attributed to the dynamic SMSI effect, which favors the formation of Zn decorated active sites (PdZn alloy or Pd modified by ZnO*x* islands) for methanol synthesis on the catalyst surface. However, the definite role of Zn in methanol synthesis and r-WGS reactions needs to be further studied.

4. Conclusions

The methanol selectivity was significantly influenced by the preparation methods and pretreatment procedures. The catalyst prepared by coprecipitation method exhibited higher methanol selectivity than those obtained from wet impregnation and deposition–precipitation methods. For the DP-catalyst, the content of PdZn alloy raised from 34% to 100% with increasing the reduction temperature from 300 °C to 500 °C, leading to the enhanced CH_3OH selectivity (from 79.4% to 85.5%). Moreover, the EXAFS results revealed that ZnO_x islands modified Pd species were formed with reducing the Pd loading, but the CH_3OH selectivity still remain the same when the reactions were conducted under similar CO_2 conversions. Therefore, we arrived at the conclusion that both the PdZn alloy and ZnO_x islands modified Pd species should be responsible for the methanol synthesis from CO_2 and hydrogen.

Acknowledgments

The authors acknowledge the financial support of the National Natural Science Foundation of China (Nos. 51271087, 21476226, 51471076, 21506204), the Key Research Programme of the CAS (KGZD-EW-T05), the Youth Innovation Promotion Association CAS, and DICP Fundamental Research Program for Clean Energy (DICPM201307). We also thank BL14W1 at Shanghai Synchrotron Radiation Facility, Shanghai institute of applied physics for the XAS experiment.

Appendix A. Supplementary data

Supplementary data associated with this article can be found, in the online version, at http://dx.doi.org/10.1016/j.apcata.2016.01.006.

References

[1] J. Graciani, K. Mudiyanselage, F. Xu, A.E. Baber, J. Evans, S.D. Senanayake, D.J. Stacchiola, P. Liu, J. Hrbek, J.F. Sanz, Science 345 (2014) 546–550.
[2] E. Ortelli, J. Wambach, A. Wokaun, Appl. Catal. A 216 (2001) 227–241.
[3] G.A. Olah, Angew. Chem. Int. Ed. 44 (2005) 2636–2639.
[4] S.G. Jadhav, P.D. Vaidya, B.M. Bhanage, J.B. Joshi, Chem. Eng. Res. Des. 92 (2014) 2557–2567.
[5] G.A. Olah, A. Goeppert, G.S. Prakash, J. Org. Chem. 74 (2008) 487–498.
[6] A. Dibenedetto, A. Angelini, P. Stufano, J. Chem. Technol. Biotechnol. 89 (2014) 334–353.
[7] C. Song, Catal. Today 115 (2006) 2–32.
[8] J. Turner, G. Sverdrup, M.K. Mann, P.C. Maness, B. Kroposki, M. Ghirardi, R.J. Evans, D. Blake, Int. J. Energy Res. 32 (2008) 379–407.
[9] M. Behrens, F. Studt, I. Kasatkin, S. Kühl, M. Hävecker, F. Abild-Pedersen, S. Zander, F. Girgsdies, P. Kurr, B.-L. Kniep, Science 336 (2012) 893–897.
[10] S. Kaluza, M. Behrens, N. Schiefenhövel, B. Kniep, R. Fischer, R. Schlögl, M. Muhler, ChemCatChem 3 (2011) 189–199.
[11] J. Bart, R. Sneeden, Catal. Today 2 (1987) 1–124.
[12] M. Spencer, Top. Catal. 8 (1999) 259–266.
[13] F. Liao, Y. Huang, J. Ge, W. Zheng, K. Tedsree, P. Collier, X. Hong, S.C. Tsang, Angew. Chem. Int. Ed. 50 (2011) 2162–2165.
[14] F. Liao, Z. Zeng, C. Eley, Q. Lu, X. Hong, S.C.E. Tsang, Angew. Chem. Int. Ed. 124 (2012) 5934–5938.
[15] F. Arena, G. Mezzatesta, G. Zafarana, G. Trunfio, F. Frusteri, L. Spadaro, J. Catal. 300 (2013) 141–151.
[16] J. Toyir, M. Saito, I. Yamauchi, S. Luo, J. Wu, I. Takahara, M. Takeuchi, Catal. Today 45 (1998) 245–250.
[17] J. Ma, N. Sun, X. Zhang, N. Zhao, F. Xiao, W. Wei, Y. Sun, Catal. Today 148 (2009) 221–231.
[18] S.E. Collins, J.J. Delgado, C. Mira, J.J. Calvino, S. Bernal, D.L. Chiavassa, M.A. Baltanás, A.L. Bonivardi, J. Catal. 292 (2012) 90–98.
[19] X. Zhou, J. Qu, F. Xu, J. Hu, J.S. Foord, Z. Zeng, X. Hong, S.C.E. Tsang, Chem. Commun. 49 (2013) 1747–1749.
[20] N. Tsubaki, K. Fujimoto, Top. Catal. 22 (2003) 325–335.
[21] T. Fujitani, I. Nakamura, Bull. Chem. Soc. Jpn. 75 (2002) 1393–1398.
[22] J. Ye, C.-J. Liu, D. Mei, Q. Ge, J. Catal. 317 (2014) 44–53.
[23] I. Melian-Cabrera, M.L. Granados, P. Terreros, J. Fierro, Catal. Today 45 (1998) 251–256.
[24] W.-J. Shen, Y. Ichihashi, H. Ando, Y. Matsumura, M. Okumura, M. Haruta, Appl. Catal. A 217 (2001) 231–239.
[25] W.-J. Shen, M. Okumura, Y. Matsumura, M. Haruta, Appl. Catal. A 213 (2001) 225–232.
[26] Y.A. Ryndin, R. Hicks, A. Bell, Y.I. Yermakov, J. Catal. 70 (1981) 287–297.
[27] T. Fujitani, M. Saito, Y. Kanai, T. Watanabe, J. Nakamura, T. Uchijima, Appl. Catal. A 125 (1995) L199–L202.
[28] N. Iwasa, H. Suzuki, M. Terashita, M. Arai, N. Takezawa, Catal. Lett. 96 (2004) 75–78.
[29] D.L. Chiavassa, S.E. Collins, A.L. Bonivardi, M.A. Baltanás, Chem. Eng. J. 150 (2009) 204–212.
[30] S.E. Collins, M.A. Baltanás, A.L. Bonivardi, J. Catal. 226 (2004) 410–421.
[31] X.-L. Liang, X. Dong, G.-D. Lin, H.-B. Zhang, Appl. Catal. B 88 (2009) 315–322.
[32] C.-H. Kim, J.S. Lee, D.L. Trimm, Stud. Surf. Sci. Catal. 153 (2004) 61–66.
[33] D. Lee, J.-Y. Lee, J.S. Lee, Stud. Surf. Sci. Catal. 153 (2004) 169–172.
[34] C.-H. Kim, J.S. Lee, D. Trimm, Top. Catal. 22 (2003) 319–324.
[35] V.M. Lebarbier, R.A. Dagle, L. Kovarik, J.A. Lizarazo-Adarme, D.L. King, D.R. Palo, Catal. Sci. Technol. 2 (2012) 2116–2127.
[36] A. Ota, E.L. Kunkes, I. Kasatkin, E. Groppo, D. Ferri, B. Poceiro, R.M.N. Yerga, M. Behrens, J. Catal. 293 (2012) 27–38.
[37] J. Wambach, A. Baiker, A. Wokaun, Phys. Chem. Chem. Phys. 1 (1999) 5071–5080.
[38] F. Cavani, F. Trifirò, A. Vaccari, Catal. Today 11 (1991) 173–301.
[39] Q. Wang, Y. Gao, Z. Zhang, L. Duan, A. Umar, D. O'Hare, Sci. Adv. Mater. 5 (2013) 411–420.
[40] Q. Wang, J. Yu, J. Liu, Z. Guo, A. Umar, L. Sun, Sci. Adv. Mater. 5 (2013) 469–474.
[41] G. Takada, R. Hidema, H. Furukawa, e-J. Surf. Sci. Nanotechnol. 10 (2012) 346–350.
[42] X. Zhao, F. Zhang, S. Xu, D.G. Evans, X. Duan, Chem. Mater. 22 (2010) 3933–3942.
[43] M.-Q. Zhao, Q. Zhang, W. Zhang, J.-Q. Huang, Y. Zhang, D.S. Su, F. Wei, J. Am. Chem. Soc. 132 (2010) 14739–14741.
[44] J. Xu, Y. Huang, X. Yang, L. He, H. Zhou, Q. Lin, T. Zhang, H. Geng, J. Nanosci. Nanotechnol. 14 (2014) 6894–6899.
[45] M. Behrens, S. Zander, P. Kurr, N. Jacobsen, J. Senker, G. Koch, T. Ressler, R.W. Fischer, R. Schl ögl, J. Am. Chem. Soc. 135 (2013) 6061–6068.
[46] M. Armbrüster, M. Behrens, K. Föttinger, M. Friedrich, É. Gaudry, S. Matam, H. Sharma, Catal. Rev. 55 (2013) 289–367.
[47] Y.-H. Chin, Y. Wang, R.A. Dagle, X.S. Li, Fuel Process. Technol. 83 (2003) 193–201.
[48] M. Friedrich, A. Ormeci, Y. Grin, M. Armbrüster, Z. Anorg, Allg. Chem. 636 (2010) 1735–1739.
[49] M. Friedrich, S. Penner, M. Heggen, M. Armbrüster, Angew. Chem. Int. Ed. 52 (2013) 4389–4392.
[50] N. Sheppard, C. De La Cruz, Catal. Today 70 (2001) 3–13.
[51] V. Lebarbier, R. Dagle, T. Conant, J.M. Vohs, A.K. Datye, Y. Wang, Catal. Lett. 122 (2008) 223–227.
[52] T. Conant, A.M. Karim, V. Lebarbier, Y. Wang, F. Girgsdies, R. Schlögl, A. Datye, J. Catal. 257 (2008) 64–70.
[53] A. Chistyakov, M. Tsodikov, V.Y. Murzin, F. Yandieva, Y.V. Zubavichus, N.Y. Kozitsyna, A. Gekhman, V. Kriventsov, I. Moiseev, Kinet. Catal. 52 (2011) 258–272.
[54] O.P. Tkachenko, A.Y. Stakheev, L.M. Kustov, I.V. Mashkovsky, M. van den Berg, W. Grünert, N.Y. Kozitsyna, Z.V. Dobrokhotova, V.I. Zhilov, S.E. Nefedov, Catal. Lett. 112 (2006) 155–161.
[55] Y. Uemura, Y. Inada, Y. Niwa, M. Kimura, K.K. Bando, A. Yagishita, Y. Iwasawa, M. Nomura, Phys. Chem. Chem. Phys. 14 (2012) 2152–2158.
[56] M.W. Tew, H. Emerich, J.A. van Bokhoven, J. Phys. Chem. C 115 (2011) 8457–8465.
[57] K. Föttinger, J.A. van Bokhoven, M. Nachtegaal, G.N. Rupprechter, J. Phys. Chem. Lett. 2 (2011) 428–433.
[58] A.I. Frenkel, C.W. Hills, R.G. Nuzzo, J. Phys. Chem. B 105 (2001) 12689–12703.
[59] N. Iwasa, S. Masuda, N. Ogawa, N. Takezawa, Appl. Catal. A 125 (1995) 145–157.

[60] N. Iwasa, T. Mayanagi, W. Nomura, M. Arai, N. Takezawa, Appl. Catal. A 248 (2003) 153–160.
[61] N. Iwasa, N. Ogawa, S. Masuda, N. Takezawa, Bull. Chem. Soc. Jpn. 71 (1998) 1451–1455.
[62] C. Amorim, M.A. Keane, J. Colloid Interface Sci. 322 (2008) 196–208.
[63] Z. Wang, M. Chen, H. Wan, Xiamen Daxue Xuebao (Ziran Kexue Ban) 50 (2011) 65–69.
[64] S.E. Collins, D.L. Chiavassa, A.L. Bonivardi, M.A. Baltanás, Catal. Lett. 103 (2005) 83–88.
[65] W. Jochum, S. Penner, R. Kramer, K. Föttinger, G. Rupprechter, B. Klötzer, J. Catal. 256 (2008) 278–286.
[66] E.L. Kunkes, F. Studt, F. Abild-Pedersen, R. Schögl, M. Behrens, J. Catal. 328 (2015) 43–48.
[67] N. Iwasa, T. Mayanagi, N. Ogawa, K. Sakata, N. Takezawa, Catal. Lett. 54 (1998) 119–123.
[68] N. Iwasa, N. Takezawa, Top. Catal. 22 (2003) 215–224.
[69] S. Lin, D. Xie, H. Guo, J. Phys. Chem. C 115 (2011) 20583–20589.